

Supporting Information for

Preparation of Co_3O_4 electrode materials with different microstructures *via* pseudomorphic conversion of Co-based metal-organic frameworks

Kyung Joo Lee,^{‡,a} Tae-Hee Kim,^{‡,b} Tae Kyung Kim,^a Jae Hwa Lee,^a Hyung-Kon Song^{*,b} and Hoi Ri Moon^{*,a}

^aDepartment of Chemistry, ^bDepartment of Energy Engineering and Department of Chemical Engineering, Ulsan National Institute of Science and Technology (UNIST), UNIST-gil 50, Ulsan 689-798, Republic of Korea.

* Corresponding authors: philphobi@hotmail.com (H.-K.S.); hoirimoon@unist.ac.kr (H.R.M.)

‡ These authors contributed equally to this work.

Table S1. X-ray crystallographic data of *p*-MOF

Compound	<i>p</i> -MOF
formula	Co ₃ C ₃₆ H ₄₀ N ₄ O ₁₆
crystal system	<i>Monoclinic</i>
space group	<i>P2(1)/n</i>
fw	961.51
<i>a</i> , Å	16.182(3)
<i>b</i> , Å	9.4700(19)
<i>c</i> , Å	16.361(3)
α , deg	90.00
β , deg	111.28(3)
γ , deg	90.00
<i>V</i> , Å ³	2336.3(8)
<i>Z</i>	2
ρ_{calcd} , g cm ⁻³	1.367
temp , K	100(2)
λ , Å	0.70002
μ , mm ⁻¹	1.017
goodness-of-fit (F^2)	0.962
$F(000)$	986
reflections collected	17122
independent reflections	4776 [$R(\text{int}) = 0.0841$]
completeness to θ_{\max} , %	99.4
data/parameters/restraints	4776/273/0
θ range for data collection, deg	2.59-26.00
diffraction limits (<i>h</i> , <i>k</i> , <i>l</i>)	-20 ≤ <i>h</i> ≤ 20, -11 ≤ <i>k</i> ≤ 11, -20 ≤ <i>l</i> ≤ 20
refinement method	Full-matrix least-squares on F^2
R_1 , wR_2 [$I > 2\sigma(I)$]	0.0801 ^a , 0.2160 ^b
R_1 , wR_2 (all data)	0.1174 ^a , 0.2357 ^b
largest peak, hole, eÅ ⁻³	1.681, -0.647

^a $R = \sum ||Fo| - |Fc|| / \sum |Fo|$. ^b $wR(F^2) = [\sum w(Fo^2 - Fc^2)^2 / \sum w(Fo^2)^2]^{1/2}$ where $w = 1 / [\sigma^2(Fo^2) + (0.1539P)^2 + (0.0000)P]$, $P = (Fo^2 + 2Fc^2)/3$.

Table S2. Selected bond distances (\AA) and angles ($^{\circ}$) of *p*-MOF

Co(1)-O(1) ^{#1}	2.059(4)	Co(1)-O(1)	2.059(4)
Co(1)-O(3) ^{#2}	2.063(4)	Co(1)-O(3) ^{#3}	2.063(4)
Co(1)-O(5) ^{#1}	2.117(4)	Co(1)-O(5)	2.117(4)
Co(2)-O(2)	2.040(4)	Co(2)-O(4) ^{#2}	2.043(4)
Co(2)-O(8)	2.067(5)	Co(2)-O(5)	2.134(4)
Co(2)-O(7)	2.189(5)	Co(2)-O(6)	2.247(5)
Co(2)-C(9)	2.517(7)	N(1)-C(13)	1.285(8)
N(1)-C(14)	1.443(10)	N(1)-C(15)	1.480(9)
N(2)-C(16)	1.337(8)	N(2)-C(18)	1.427(9)
N(2)-C(17)	1.447(9)	O(1)-C(1)	1.257(7)
O(2)-C(1)	1.238(8)	O(3)-C(8)	1.255(8)
O(3)-Co(1) ^{#4}	2.063(4)	O(4)-C(8)	1.262(7)
O(4)-Co(2) ^{#5}	2.043(4)	O(5)-C(9)	1.252(8)
O(6)-C(9)	1.243(8)	O(7)-C(13)	1.242(7)
O(8)-C(16)	1.227(8)	C(1)-C(2)	1.521(8)
C(2)-C(7)	1.361(9)	C(2)-C(3)	1.403(8)
C(3)-C(4)	1.387(9)	C(4)-C(5)	1.375(9)
C(5)-C(6)	1.379(9)	C(5)-C(8)	1.508(9)
C(6)-C(7)	1.398(9)	C(9)-C(10)	1.601(11)
C(10)-C(11)	1.374(10)	C(10)-C(12) ^{#6}	1.375(10)
C(11)-C(12)	1.381(11)	C(12)-C(10) ^{#6}	1.375(10)
O(1) ^{#1} -Co(1)-O(1)	179.999(1)	O(1) ^{#1} -Co(1)-O(3) ^{#2}	85.23(18)
O(1)-Co(1)-O(3) ^{#2}	94.77(18)	O(1) ^{#1} -Co(1)-O(3) ^{#3}	94.77(18)
O(1)-Co(1)-O(3) ^{#3}	85.23(18)	O(3) ^{#2} -Co(1)-O(3) ^{#3}	180
O(1) ^{#1} -Co(1)-O(5) ^{#1}	89.84(17)	O(1)-Co(1)-O(5) ^{#1}	90.16(17)
O(3) ^{#2} -Co(1)-O(5) ^{#1}	91.12(17)	O(3) ^{#3} -Co(1)-O(5) ^{#1}	88.88(17)
O(1) ^{#1} -Co(1)-O(5)	90.16(17)	O(1)-Co(1)-O(5)	89.84(17)
O(3) ^{#2} -Co(1)-O(5)	88.88(18)	O(3) ^{#3} -Co(1)-O(5)	91.13(17)

O(5) ^{#1} -Co(1)-O(5)	180	O(2)-Co(2)-O(4) ^{#2}	99.47(17)
O(2)-Co(2)-O(8)	88.01(18)	O(4) ^{#2} -Co(2)-O(8)	97.65(18)
O(2)-Co(2)-O(5)	97.97(18)	O(4) ^{#2} -Co(2)-O(5)	97.92(17)
O(8)-Co(2)-O(5)	162.15(18)	O(2)-Co(2)-O(7)	173.61(17)
O(4) ^{#2} -Co(2)-O(7)	86.44(17)	O(8)-Co(2)-O(7)	88.80(18)
O(5)-Co(2)-O(7)	83.52(17)	O(2)-Co(2)-O(6)	93.25(17)
O(4) ^{#2} -Co(2)-O(6)	155.42(17)	O(8)-Co(2)-O(6)	103.77(19)
O(5)-Co(2)-O(6)	59.29(17)	O(7)-Co(2)-O(6)	82.14(17)
O(2)-Co(2)-C(9)	97.9(2)	O(4) ^{#2} -Co(2)-C(9)	126.9(2)
O(8)-Co(2)-C(9)	132.9(2)	O(5)-Co(2)-C(9)	29.8(2)
O(7)-Co(2)-C(9)	80.3(2)	O(6)-Co(2)-C(9)	29.55(19)
C(13)-N(1)-C(14)	119.6(6)	C(13)-N(1)-C(15)	121.0(7)
C(14)-N(1)-C(15)	119.3(6)	C(16)-N(2)-C(18)	121.7(6)
C(16)-N(2)-C(17)	121.6(6)	C(18)-N(2)-C(17)	116.7(6)
C(1)-O(1)-Co(1)	138.4(4)	C(1)-O(2)-Co(2)	129.7(4)
C(8)-O(3)-Co(1) ^{#4}	140.5(4)	C(8)-O(4)-Co(2) ^{#5}	124.2(4)
C(9)-O(5)-Co(1)	133.2(4)	C(9)-O(5)-Co(2)	92.3(4)
Co(1)-O(5)-Co(2)	111.84(18)	C(9)-O(6)-Co(2)	87.4(4)
C(13)-O(7)-Co(2)	119.9(4)	C(16)-O(8)-Co(2)	126.1(4)
O(2)-C(1)-O(1)	127.7(6)	O(2)-C(1)-C(2)	117.5(5)
O(1)-C(1)-C(2)	114.7(6)	C(7)-C(2)-C(3)	120.2(6)
C(7)-C(2)-C(1)	119.2(6)	C(3)-C(2)-C(1)	120.6(6)
C(4)-C(3)-C(2)	119.0(6)	C(5)-C(4)-C(3)	121.6(6)
C(4)-C(5)-C(6)	118.3(6)	C(4)-C(5)-C(8)	121.1(6)
C(6)-C(5)-C(8)	120.5(6)	C(5)-C(6)-C(7)	121.4(7)
C(2)-C(7)-C(6)	119.5(6)	O(3)-C(8)-O(4)	126.3(6)
O(3)-C(8)-C(5)	116.9(5)	O(4)-C(8)-C(5)	116.8(6)
O(6)-C(9)-O(5)	120.8(6)	O(6)-C(9)-C(10)	122.9(6)
O(5)-C(9)-C(10)	115.9(6)	O(6)-C(9)-Co(2)	63.1(4)
O(5)-C(9)-Co(2)	57.9(3)	C(10)-C(9)-Co(2)	167.6(5)

C(11)-C(10)-C(12) ^{#6}	122.9(8)	C(11)-C(10)-C(9)	119.8(6)
C(12) ^{#6} -C(10)-C(9)	117.3(7)	C(10)-C(11)-C(12)	118.8(7)
C(10) ^{#6} -C(12)-C(11)	118.2(7)	O(7)-C(13)-N(1)	125.5(7)
O(8)-C(16)-N(2)	126.2(7)		

Symmetry transformation used to generate equivalent atoms:

^{#1}, -x+1, -y+2, -z; ^{#2}, x-1/2, -y+5/2, z-1/2; ^{#3}, -x+3/2, y-1/2, -z+1/2; ^{#4}, -x+3/2, y+1/2, -z+1/2;
^{#5}, x+1/2, -y+5/2, z+1/2; ^{#6}, -x+1, -y+1, -z.

Table S3. X-ray crystallographic data of *r*-MOF

Compound	<i>r</i> -MOF
formula	Co ₂ C ₂₀ H ₂₀ S ₂ O ₁₀
crystal system	<i>Triclinic</i>
space group	<i>P-1</i>
fw	602.34
<i>a</i> , Å	7.3489(15)
<i>b</i> , Å	10.969(2)
<i>c</i> , Å	16.002(3)
α , deg	72.51(3)
β , deg	78.52(3)
γ , deg	73.12(3)
<i>V</i> , Å ³	1168.5(4)
<i>Z</i>	2
ρ_{calcd} , g cm ⁻³	1.712
temp , K	173(2)
λ , Å	0.71073
μ , mm ⁻¹	1.652
goodness-of-fit (<i>F</i> ²)	1.183
<i>F</i> (000)	612
reflections collected	11151
independent reflections	5300 [<i>R</i> (int) = 0.0983]
completeness to θ_{\max} , %	99.8
data/parameters/restraints	5300/311/0
θ range for data collection, deg	3.02-27.48
diffraction limits (<i>h</i> , <i>k</i> , <i>l</i>)	-9 ≤ <i>h</i> ≤ 9, -14 ≤ <i>k</i> ≤ 14, -20 ≤ <i>l</i> ≤ 20
refinement method	Full-matrix least-squares on <i>F</i> ²
<i>R</i> ₁ , <i>wR</i> ₂ [<i>I</i> >2σ(<i>I</i>)]	0.1242 ^a , 0.3121 ^b
<i>R</i> ₁ , <i>wR</i> ₂ (all data)	0.1750 ^a , 0.3591 ^b
largest peak, hole, eÅ ⁻³	6.444, -1.655

^a $R = \sum ||Fo| - |Fc|| / \sum |Fo|$. ^b $wR(F^2) = [\sum w(Fo^2 - Fc^2)^2 / \sum w(Fo^2)^2]^{1/2}$ where $w = 1 / [\sigma^2(Fo^2) + (0.2000P)^2 + (0.0000)P]$, $P = (Fo^2 + 2Fc^2)/3$.

Table S4. Selected bond distances (\AA) and angles ($^{\circ}$) of *r*-MOF

Co(1)-O(1)	2.041(7)	Co(1)-O(6) ^{#1}	2.047(7)
Co(1)-O(8) ^{#2}	2.051(7)	Co(1)-O(3)	2.051(6)
Co(1)-O(1D)	2.195(7)	Co(1)-O(2D)	2.213(6)
Co(2)-O(7)	2.041(7)	Co(2)-O(2)	2.055(7)
Co(2)-O(4)	2.055(7)	Co(2)-O(5) ^{#3}	2.058(7)
Co(2)-O(2D)	2.212(6)	Co(2)-O(1D) ^{#4}	2.218(7)
O(1)-C(1)	1.248(12)	O(2)-C(1)	1.262(12)
O(3)-C(5)	1.251(12)	O(4)-C(5)	1.230(12)
O(5)-C(12)	1.216(12)	O(5)-Co(2) ^{#5}	2.058(7)
O(6)-C(12)	1.261(12)	O(6)-Co(1) ^{#6}	2.047(7)
O(7)-C(13)	1.248(12)	O(8)-C(13)	1.266(12)
O(8)-Co(1) ^{#4}	2.051(7)	C(1)-C(2)	1.504(13)
C(2)-C(3)	1.383(15)	C(2)-C(4)	1.391(15)
C(3)-C(4) ^{#7}	1.365(15)	C(4)-C(3) ^{#7}	1.365(15)
C(5)-C(6)	1.517(12)	C(6)-C(7)	1.368(15)
C(6)-C(11)	1.392(14)	C(7)-C(8)	1.393(15)
C(8)-C(9)	1.405(15)	C(9)-C(10)	1.388(16)
C(9)-C(12)	1.507(13)	C(10)-C(11)	1.378(14)
C(13)-C(14)	1.518(14)	C(14)-C(15)	1.346(17)
C(14)-C(16)	1.398(16)	C(15)-C(16) ^{#8}	1.400(16)
C(16)-C(15) ^{#8}	1.400(16)	S(1)-O(1D)	1.536(6)
S(1)-C(17)	1.753(18)	S(1)-C(18)	1.777(16)
O(1D)-Co(2) ^{#2}	2.218(7)	S(2)-O(2D)	1.529(6)
S(2)-C(20)	1.712(17)	S(2)-C(19)	1.765(16)
O(1)-Co(1)-O(6) ^{#1}	85.0(3)	O(1)-Co(1)-O(8) ^{#2}	177.8(3)
O(6) ^{#1} -Co(1)-O(8) ^{#2}	95.6(3)	O(1)-Co(1)-O(3)	94.6(3)
O(6) ^{#1} -Co(1)-O(3)	177.6(3)	O(8) ^{#2} -Co(1)-O(3)	84.8(3)
O(1)-Co(1)-O(1D)	84.6(3)	O(6) ^{#1} -Co(1)-O(1D)	91.0(3)

O(8) ^{#2} -Co(1)-O(1D)	93.2(3)	O(3)-Co(1)-O(1D)	86.5(3)
O(1)-Co(1)-O(2D)	89.3(3)	O(6) ^{#1} -Co(1)-O(2D)	92.9(3)
O(8) ^{#2} -Co(1)-O(2D)	92.9(3)	O(3)-Co(1)-O(2D)	89.5(3)
O(1D)-Co(1)-O(2D)	172.4(2)	O(7)-Co(2)-O(2)	177.4(3)
O(7)-Co(2)-O(4)	85.4(3)	O(2)-Co(2)-O(4)	95.4(3)
O(7)-Co(2)-O(5) ^{#3}	94.4(3)	O(2)-Co(2)-O(5) ^{#3}	84.8(3)
O(4)-Co(2)-O(5) ^{#3}	179.4(3)	O(7)-Co(2)-O(2D)	85.2(3)
O(2)-Co(2)-O(2D)	92.4(3)	O(4)-Co(2)-O(2D)	91.9(3)
O(5) ^{#3} -Co(2)-O(2D)	87.5(3)	O(7)-Co(2)-O(1D) ^{#4}	88.4(3)
O(2)-Co(2)-O(1D) ^{#4}	94.1(3)	O(4)-Co(2)-O(1D) ^{#4}	91.3(3)
O(5) ^{#3} -Co(2)-O(1D) ^{#4}	89.3(3)	O(2D)-Co(2)-O(1D) ^{#4}	172.5(2)
C(1)-O(1)-Co(1)	134.5(7)	C(1)-O(2)-Co(2)	131.7(7)
C(5)-O(3)-Co(1)	137.0(6)	C(5)-O(4)-Co(2)	130.4(7)
C(12)-O(5)-Co(2) ^{#5}	132.2(7)	C(12)-O(6)-Co(1) ^{#6}	132.9(6)
C(13)-O(7)-Co(2)	139.2(7)	C(13)-O(8)-Co(1) ^{#4}	127.5(6)
O(1)-C(1)-O(2)	126.9(9)	O(1)-C(1)-C(2)	116.3(9)
O(2)-C(1)-C(2)	116.6(9)	C(3)-C(2)-C(4)	117.0(9)
C(3)-C(2)-C(1)	121.4(9)	C(4)-C(2)-C(1)	121.5(9)
C(4) ^{#7} -C(3)-C(2)	123.0(10)	C(3) ^{#7} -C(4)-C(2)	119.9(10)
O(4)-C(5)-O(3)	126.5(9)	O(4)-C(5)-C(6)	117.8(9)
O(3)-C(5)-C(6)	115.7(9)	C(7)-C(6)-C(11)	119.7(9)
C(7)-C(6)-C(5)	120.2(9)	C(11)-C(6)-C(5)	120.1(9)
C(6)-C(7)-C(8)	121.5(10)	C(7)-C(8)-C(9)	119.0(11)
C(10)-C(9)-C(8)	118.6(9)	C(10)-C(9)-C(12)	121.0(9)
C(8)-C(9)-C(12)	120.4(10)	C(11)-C(10)-C(9)	121.7(11)
C(10)-C(11)-C(6)	119.4(11)	O(5)-C(12)-O(6)	126.5(9)
O(5)-C(12)-C(9)	117.0(8)	O(6)-C(12)-C(9)	116.4(9)
O(7)-C(13)-O(8)	125.4(9)	O(7)-C(13)-C(14)	115.7(9)
O(8)-C(13)-C(14)	118.8(9)	C(15)-C(14)-C(16)	120.6(10)
C(15)-C(14)-C(13)	119.6(10)	C(16)-C(14)-C(13)	119.7(11)

C(14)-C(15)-C(16) ^{#8}	121.8(12)	C(14)-C(16)-C(15) ^{#8}	117.5(12)
O(1D)-S(1)-C(17)	106.8(6)	O(1D)-S(1)-C(18)	105.0(7)
C(17)-S(1)-C(18)	102.5(13)	S(1)-O(1D)-Co(1)	111.8(4)
S(1)-O(1D)-Co(2) ^{#2}	135.3(4)	Co(1)-O(1D)-Co(2) ^{#2}	112.9(3)
O(2D)-S(2)-C(20)	104.8(6)	O(2D)-S(2)-C(19)	105.8(6)
C(20)-S(2)-C(19)	100.5(12)	S(2)-O(2D)-Co(2)	111.5(4)
S(2)-O(2D)-Co(1)	135.6(4)	Co(2)-O(2D)-Co(1)	112.8(3)

Symmetry transformation used to generate equivalent atoms:

^{#1}, x, y+1, z; ^{#2}, x+1, y, z; ^{#3}, x-1, y+1, z; ^{#4}, x-1, y, z; ^{#5}, x+1, y-1, z; ^{#6}, x, y-1, z;
^{#7}, -x, -y+1, -z+1; ^{#8}, -x, -y, -z.

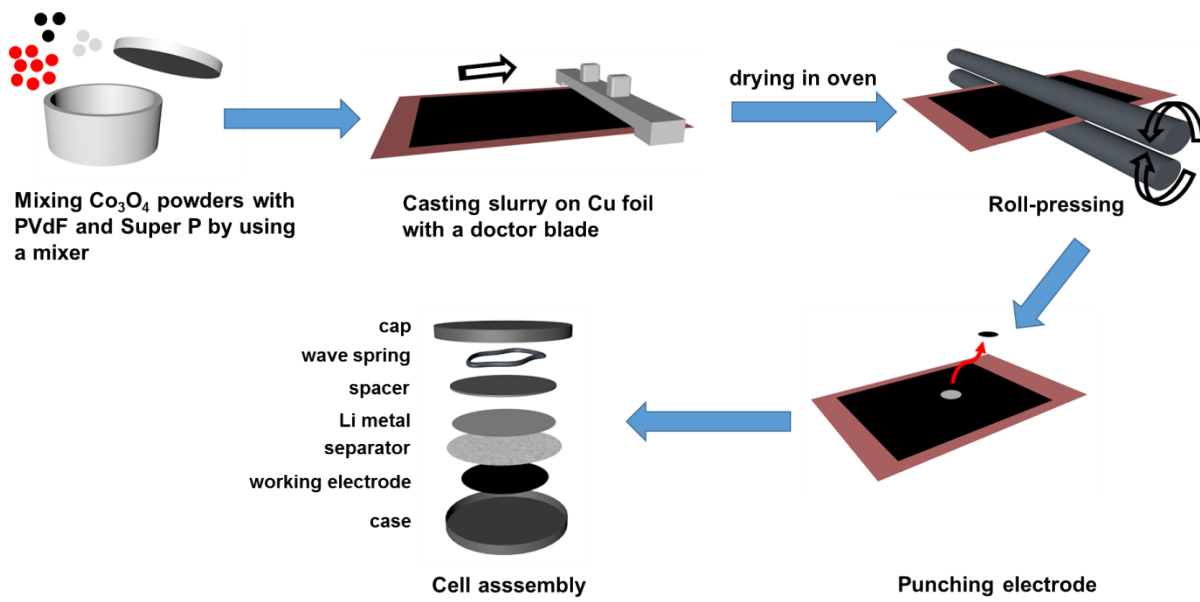


Fig. S1 Fabrication of a coin-type half-cell in an Ar-filled glove box.

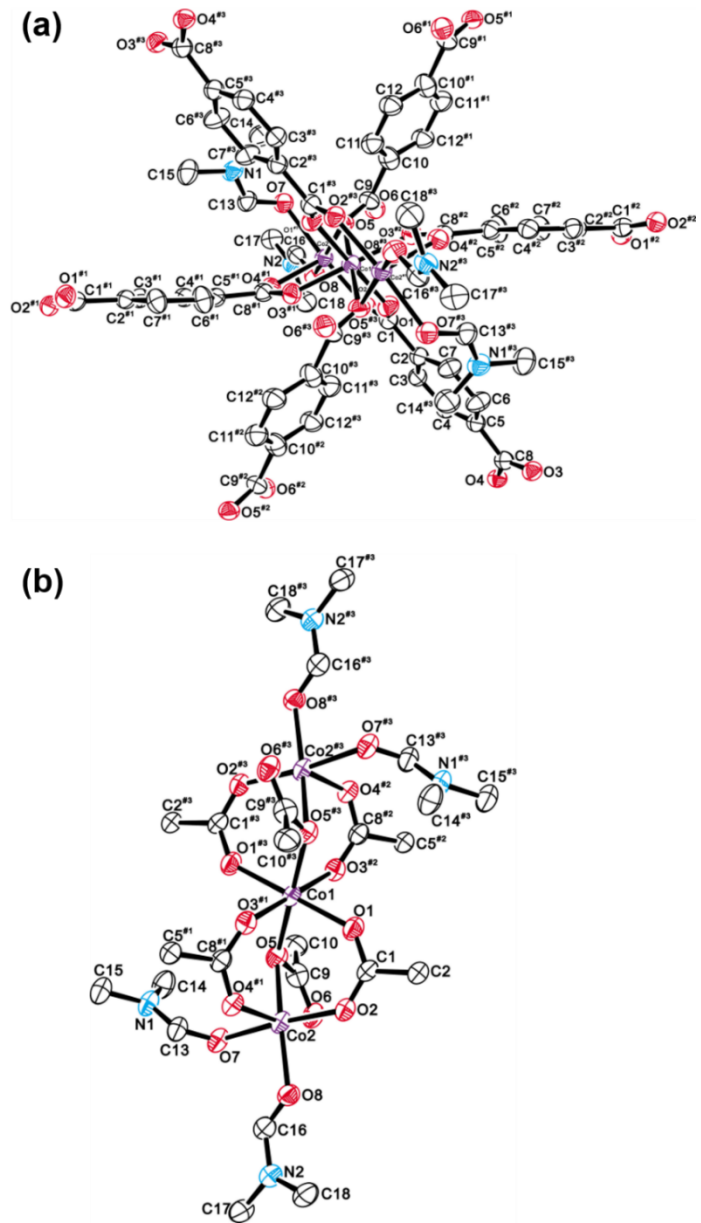


Fig. S2 An ORTEP drawing of *p*-MOF with an atomic numbering scheme (thermal ellipsoids at 30% probability). (a) A shot for arrangement of ligands around the central cobalt atoms, and (b) a shot showing the coordination modes of the cobalt atoms. Hydrogen atoms are omitted for clarity. Symmetry operations: ${}^{\#1}$, x , $y+1$, z ; ${}^{\#2}$, $x-1/2$, $-y+5/2$, $z-1/2$; ${}^{\#3}$, $-x+1$, $-y+2$, $-z$. Co, purple; C, gray; N, blue; O, red.

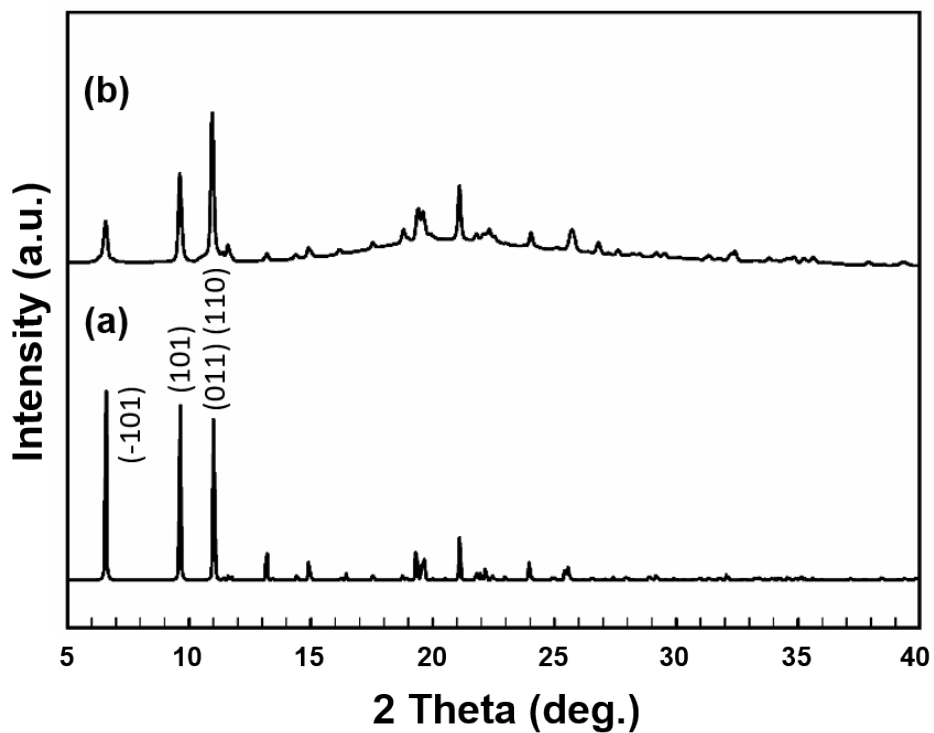


Fig. S3 XRPD patterns of *p*-MOF. (a) Simulated pattern from single-crystal XRD data, and (b) experimental pattern of as-synthesized *p*-MOF.

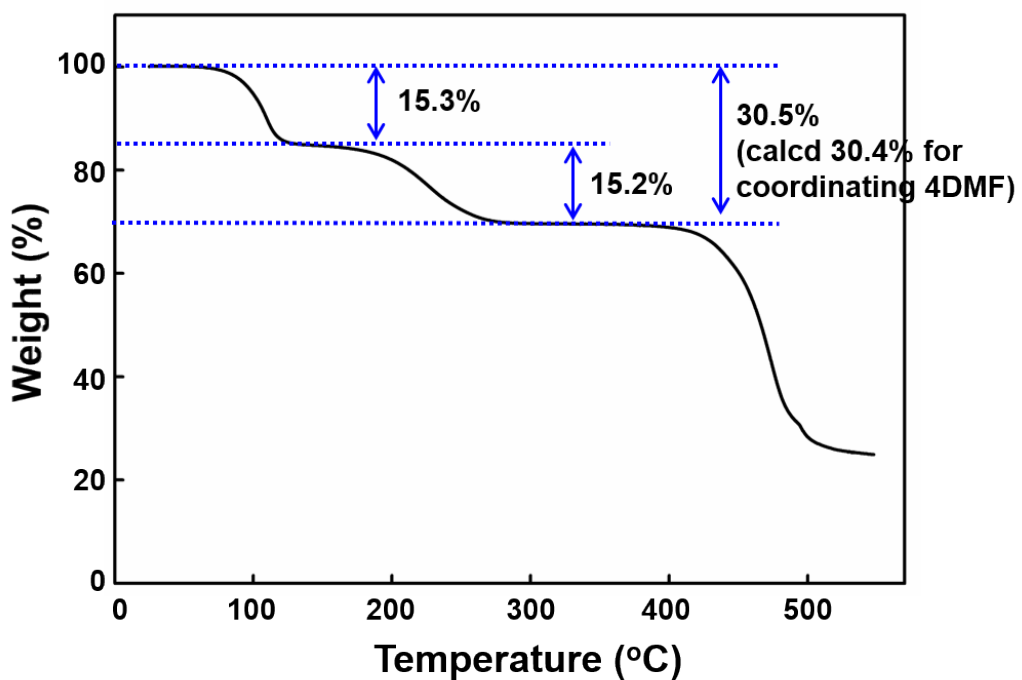


Fig. S4 TGA trace of $[\text{Co}_3(\text{BDC})_3(\text{DMF})_4]_n$ (*p*-MOF). The result indicates that 30.5% weight loss at 80 – 350 °C, corresponding to the loss of 4 DMF molecules (calc. 30.4%), followed by additional weight loss at ~440 °C, corresponding to decomposition of *p*-MOF.

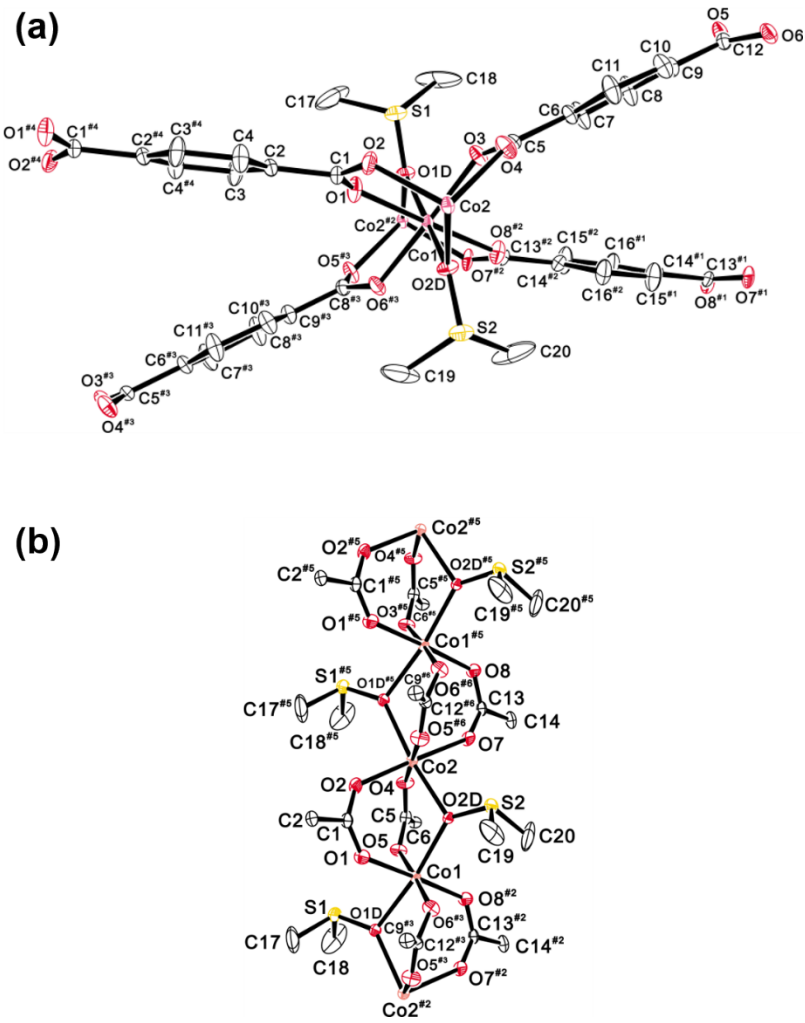


Fig. S5 ORTEP drawings of *r*-MOF with an atomic numbering scheme (thermal ellipsoids at 30% probability). (a) A shot for arrangement of ligands around the central cobalt atoms, and (b) a shot showing the coordination modes of the cobalt atoms. Hydrogen atoms are omitted for clarity. Symmetry operations: ${}^{\#1}$, $-x+1, -y, -z$; ${}^{\#2}$, $x+1, y, z$; ${}^{\#3}$, $x, y+1, z$; ${}^{\#4}$, $x, y+1, z+1$; ${}^{\#5}$, $x-1, y, z$; ${}^{\#6}$, $x-1, y+1, z$. Co, pink; C, gray; S, yellow; O, red.

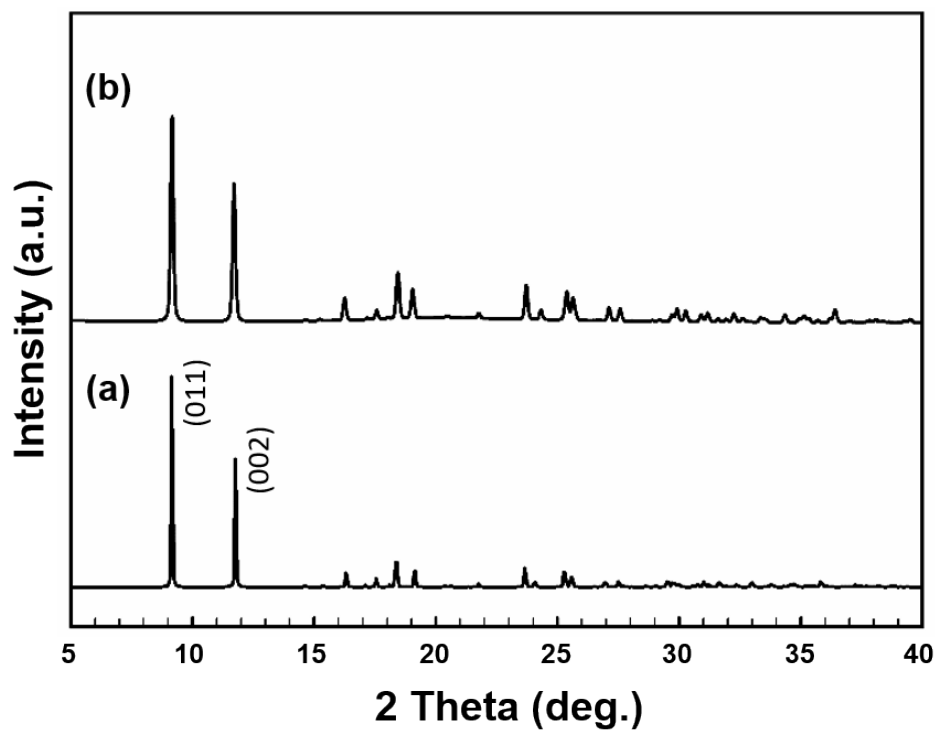


Fig. S6 XRPD patterns of *r*-MOF. (a) Simulated pattern from single-crystal XRD data, and (b) experimental pattern of as-synthesized *r*-MOF.

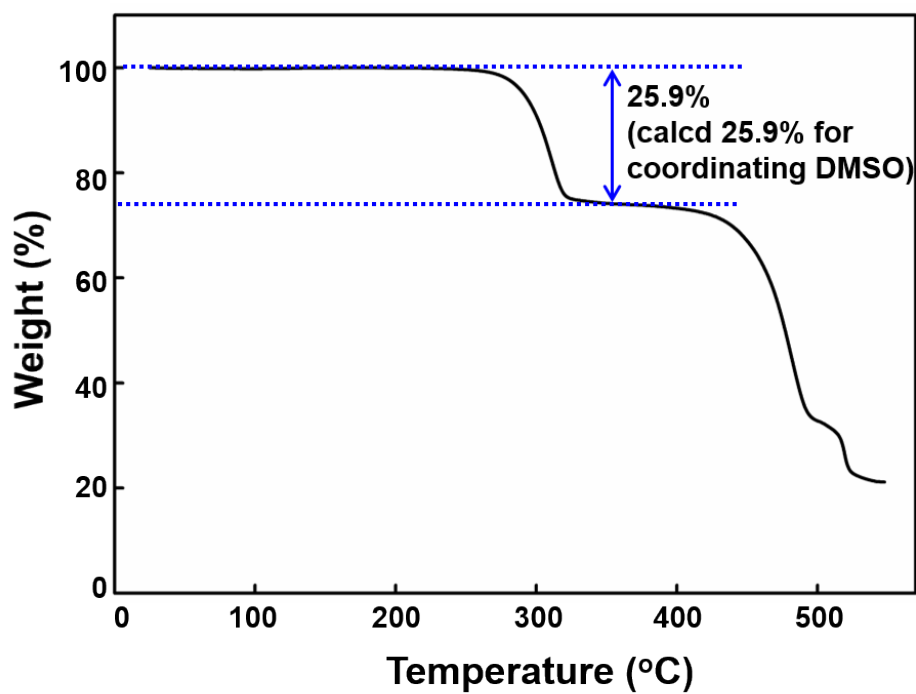


Fig. S7 TGA trace of $[\text{Co}(\text{BDC})(\text{DMSO})]_n$ (*r*-MOF). The result indicates that 25.9% weight loss at 250 – 330 °C, corresponding to the loss of a DMSO molecule (calc. 25.9%), followed by additional weight loss above ~500 °C, corresponding to decomposition of *r*-MOF.

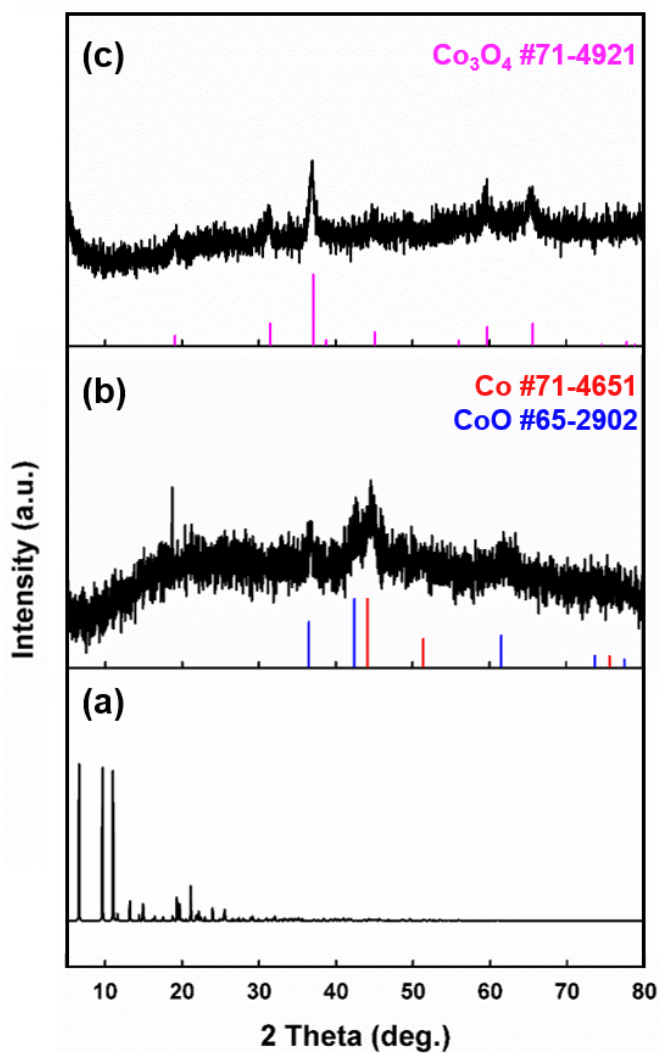


Fig. S8 XRPD patterns of *p*-MOF and products obtained after heat treatments. (a) Simulated pattern from single-crystal XRD data, (b) sample after the first thermal treatment under a nitrogen flow with red lines and blue lines indicating the reported values of Co (JCPDS file No. 71-4651) and CoO (JCPDS file No. 65-2902), respectively, and (c) sample after the second thermal treatment under an oxygen flow with pink lines indicating the reported values of Co₃O₄ (JCPDS file No. 71-4921).

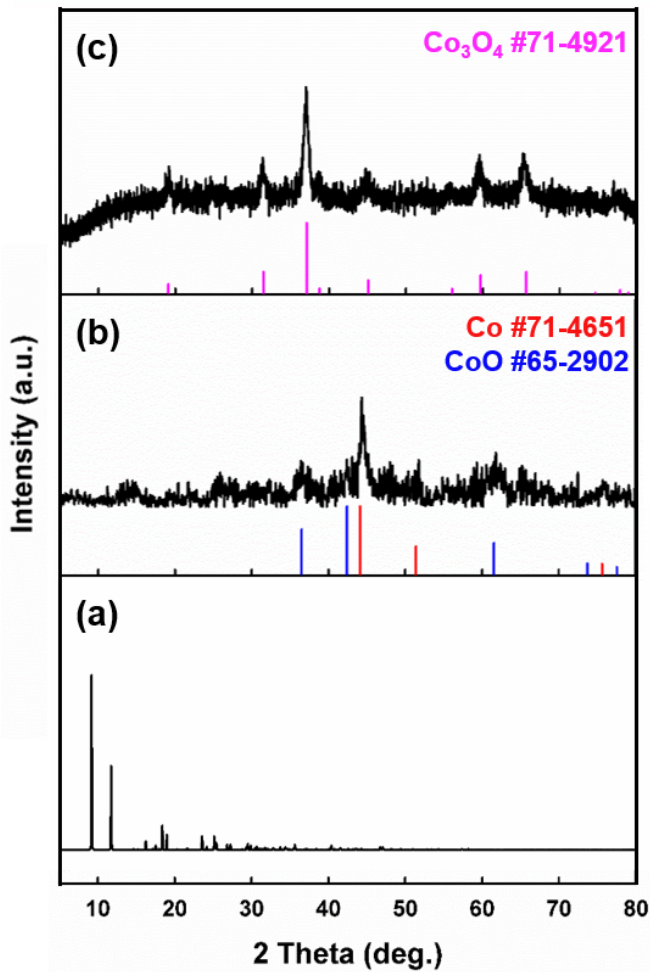


Fig. S9 XRPD patterns of *r*-MOF and products obtained after heat treatments. (a) Simulated pattern from single-crystal XRD data, (b) sample after the first thermal treatment under a nitrogen flow with red lines and blue lines indicating the reported values of Co (JCPDS file No. 71-4651) and CoO (JCPDS file No. 65-2902), respectively, and (c) sample after the second thermal treatment under an oxygen flow with pink lines indicating the reported values of Co₃O₄ (JCPDS file No. 71-4921).

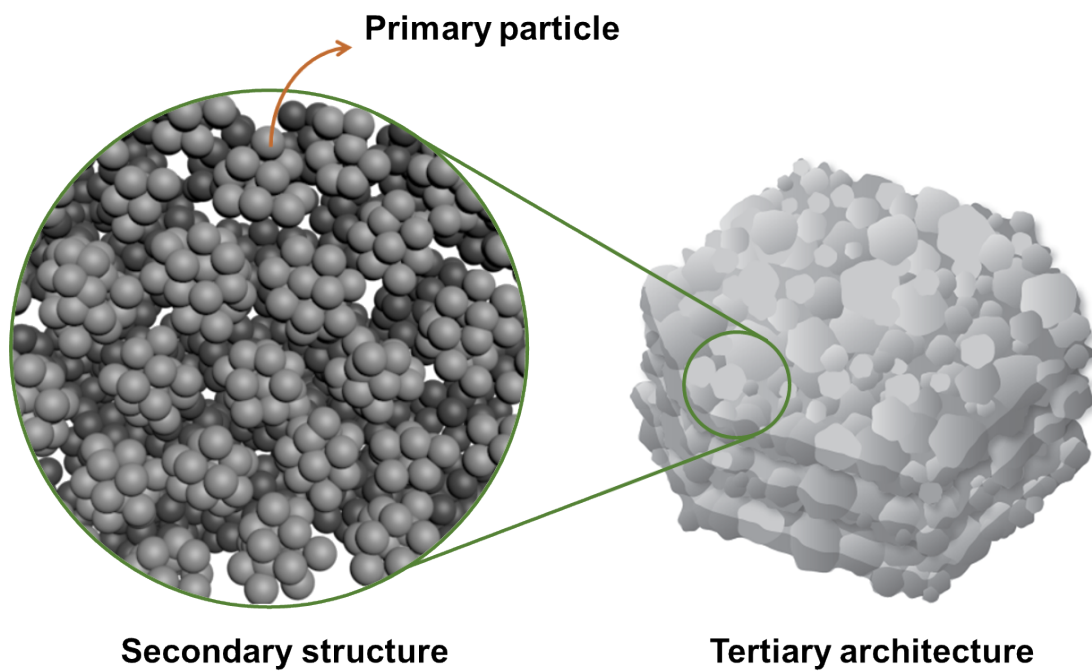


Fig. S10 Illustration of a hierarchical structure in Co_3O_4 nanomaterials. Within $p\text{-Co}_3\text{O}_4$ and $r\text{-Co}_3\text{O}_4$ nearly identical primary particles are agglomerated to form the secondary structures (100 to 300 nm), which finally construct the macroscopic tertiary architectures.

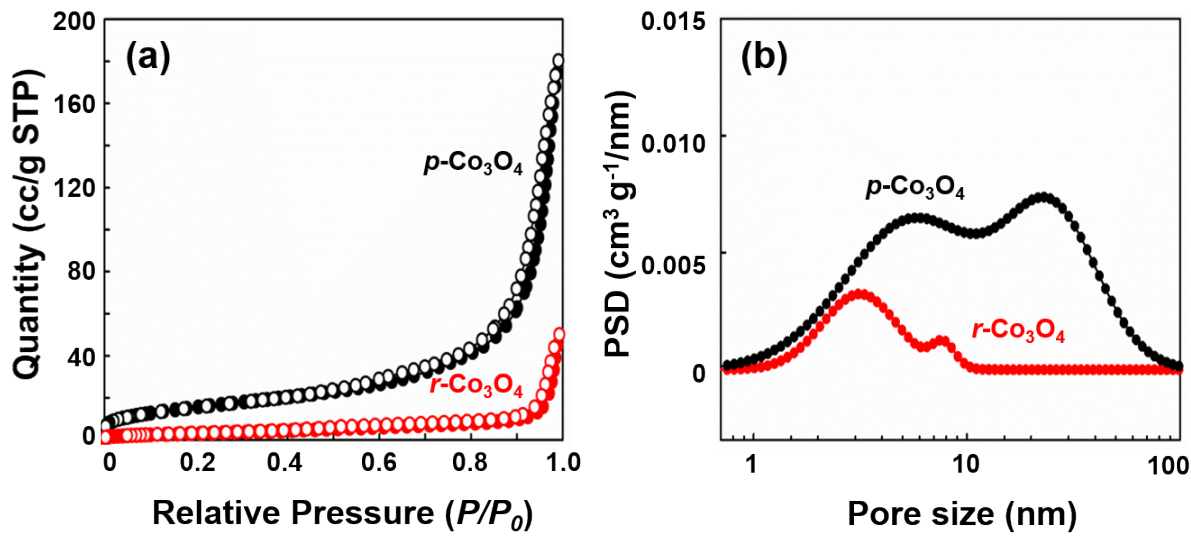


Fig. S11 (a) N_2 sorption isotherms and (b) NLDFT pore size distribution curve of $p\text{-Co}_3\text{O}_4$ as black one and $r\text{-Co}_3\text{O}_4$ as red one.

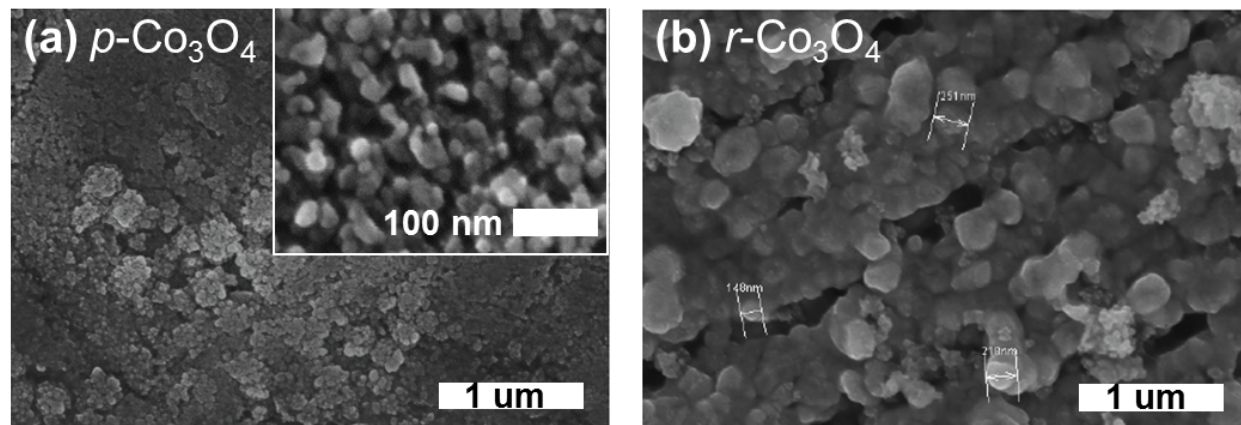


Fig. S12 SEM images of composite electrodes containing (a) $p\text{-Co}_3\text{O}_4$ and (b) $r\text{-Co}_3\text{O}_4$. The interconnected secondary particles is clearly shown in (b) while the primary particles agglomerates without connectivity between them recognized in (a).